Modeling of GPS total electron content over the African low latitude region using empirical orthogonal functions

Geoffrey Andima[1], Emirant B Amabayo[1,2], Edward Jurua[1], and Pierre J Cilliers[3]

[1]Department of Physics, Mbarara University of Science and Technology, Mbarara, Uganda
[2]Department of Physics, Busitema University, Tororo, Uganda
[3]South African National Space Agency (SANSA) Space Science, Hermanus, South Africa

Correspondence: Geoffrey Andima (geoffrey.andima@gmail.com)

Abstract. In this paper, an empirical total electron content (TEC) model and trends in TEC over the African low latitude region are presented. GPS-derived TEC data from Malindi, Kenya (geographic coordinates 40.194^oE, 2.996^oS) and global ionospheric maps (GIMs) were used. We employed empirical orthogonal function (EOF) analysis method together with least square regression to model the TEC. The EOF-based TEC model was validated through comparisons with GIMs, GPS-derived TEC and TEC derived from the International Reference Ionosphere-2016 (IRI-2016) model for selected quiet and storm conditions. The single station EOF-based TEC model over Malindi satisfactorily reproduced the known diurnal, semiannual and annual variations in the TEC. Comparison of the EOF-based TEC model results with TEC derived from IRI-2016 model showed that the EOF-based model predicted the TEC over Malindi with smaller errors than the IRI-2016. For the selected storms, the EOF-based TEC model simulated the storm time TEC response over Malindi better than the IRI-2016. In the case of the regional model, the EOF-based TEC model was able to reproduce the TEC characteristics in the equatorial ionization anomaly region. The EOF-based TEC model was then used as a background in estimating TEC trends. A latitudinal dependence in the trends was observed over the African low latitude region.

1 Introduction

The features of the low latitude ionosphere are quite unique. During daytime, a double peaked ionization structure appears over the low latitude region, a phenomenon often referred to as the equatorial ionization anomaly (EIA). The EIA is normally explained in terms of the plasma fountain theory (Martyn, 1947; Moffett, 1979). The daytime E region eastward electric field in combination with the nearly horizontal Earth's magnetic field generate a large vertically directed E×B drift force at the dip equator that raises the plasma to higher altitudes. The raised plasma diffuses away from the geomagnetic equator under gravity and pressure gradient forces along the equipotential magnetic field lines to form ionization peaks at dip latitudes $\sim \pm 15^o$, and a trough that extends over the dip equator (Appleton, 1946). Prior to the electric field turning westwards at night, it is enhanced (prereversal enhancement (PRE)) resulting in plasma uplift into regions of low recombination. Associated with the electron density at the EIA enhancement is a density gradient instability of the Rayleigh Taylor (RT) type which creates a spectrum of plasma irregularities that fill the post sunset low latitude ionosphere (Kelley, 2009). The EIA and the PRE vary with location,

solar activity, season, and even on daily basis. These variations make it difficult to predict the characteristics of the low latitude ionosphere.

The state of the ionosphere is of great importance in space based navigation systems such as the Global Navigation Satellite Systems (GNSS). The total electron content (TEC) is of particular interest to users of GNSS systems. For many practical pur-
5   poses in the GPS, the desired ionospheric parameter is the TEC. This is because many of the effects on transionospheric satellite links (e.g time delay, Polarization, Faraday rotation, Doppler shift) are related to TEC in one way or another (Kersley et al., 2004). The low latitude ionosphere exhibits the highest values of TEC globally. Therefore, pronounced ionospheric effects are experienced by radio signals transiting the low latitude ionosphere. Understanding the low latitude ionospheric dynamics in a bid to forecast its day to day conditions is key for advancement of space technology and the improvement of GNSS accuracy.
10   Ionospheric variability over the low latitude region of Africa, based on TEC analysis, has been reported before (e.g Adewale et al. 2011; Olwendo et al. 2012; Habarulema et al. 2013; Andima et al. 2015). From these studies, the diurnal, seasonal, disturbed and quiet time TEC characteristics over the region have been revealed. However, these analyses made use of TEC data of either the same solar phase or the same solar cycle. With now a relatively longer record of data in the achieves, it is imperative to extend these studies to the long-term TEC characteristics over the African low latitude region for practical applications.
15   A common approach to TEC prediction is through modeling. Various TEC models (e.g Anderson et al. 1987; Rawer and Bilitza 1990; Reinisch et al. 2004; Lean et al. 2011; Hajra et al. 2016; Ercha et al. 2012; Chen et al. 2015; Ercha et al. 2012) have been developed; however, many of these models are limited in geographical extend. A widely used model to describe the global TEC climatology is the Intenational Reference Ionosphere (IRI) model (Bilitza, 1990). The IRI is an empirical model synthesized from global data sets comprising of ionosonde, radar and in situ measurements (Bilitza, 1990; Rawer and Bilitza, 1990). Av-
20   eraging and smoothing applied when deriving the model coefficients may limit its accuracy in capturing peculiar features such as the TEC variability in the EIA region. Under such circumstances, regional models are superior in characterizing the background TEC.

Long term trends in ionospheric parameters are indicative of the deviation in the ionospheric parameters from their background values. Ionospheric trends are important in understanding the changes in Earth's energy balance (Elias, 2011). Various
25   studies (e.g Jarvis et al. 1998; Bencze 2002, 2005; Lastovicka et al. 2006; Danilov and Mikhailov 1999; Bremer et al. 2012) have reported on long-term trends in ionospheric parameters derived from ionosonde data. A conclusion from these studies is that trends in the F2 layer critical frequency (foF2) and F2 layer maximum electron density height (hmF2) are negative. Some studies on ionospheric trends have also revealed latitudinal dependence of these trends (Danilov and Mikhailov, 1999). Lean et al. (2011) using a database of global ionospheric maps (GIMs) reported that global TEC trends are positive and are
30   dependent on the geomagnetic latitude. Also cases of negligible or no trends in TEC have been observed. For instance, results obtained by Lastovicka et al. (2017) show a weak negative or no trend in ionospheric TEC. Despite the various studies on trends of different ionospheric parameters, those relating to TEC remain limited, and hence the question on the nature of ionospheric TEC trends still need to be answered. There is a need to investigate whether TEC has negative (Lastovicka et al., 2017), or positive (Lean et al., 2011), or no (Lastovicka, 2013) trend. The objective of this paper is therefore two fold: first to

attempt to model low latitude TEC and secondly to estimate trends in the variation of the ionospheric TEC over the African low latitude region using actual TEC measurements by means of regional GPS receivers, and data from the GIMs.

2   Data sets used

The International GNSS Service (IGS) operates a number of GPS ground based receivers over the African low latitude region. In this study, data was obtained from one of the IGS receivers located at Malindi, Kenya which archived data from 1995 to date (December 2017). Prior to 2008, the IGS receiver (station code MALI) was installed at 40.19439^o E, 2.99591^oS and then replaced with another (station code MAL2) installed at 40.19414^oE, 2.99606^oS. These receivers had nearly the same location and therefore sampled the same geographical region of the ionosphere. We obtained the Receiver Independent EXchange (RINEX) files from ftp://cddis.gsfc.nasa.gov/ and then extracted the TEC along the line-of-site, slant TEC (sTEC), from the RINEX files using the GPS-TEC software of Boston College (Seemala and Valladares, 2011). This software uses the thin shell mapping function to map the sTEC to the vertical to obtain the vertical TEC (vTEC) at an assumed ionospheric height of 350 km. The vTEC for the different viewing geometries for satellites with elevation angles greater than 30° were averaged epoch-by-epoch to give a representation of the vTEC above the receiver. Due to data paucity from 1995 to 1998, only data from 1999 to 2017 were used in this study. Hourly averages of the daily TEC data were then calculated to minimize noise in the data. The hourly averages were organized into a data matrix $M_{d \times h}$ (day×hour) which was used to model and estimate trends in TEC over Malindi. To study the TEC over the African low latitude region, TEC from the GIMs, a reliable source of ionospheric data (Hernandez-Pajares et al., 2009), was used. Though these maps have been available since 1998, for comparison purposes with the GPS data, we have used data from 1999-2017. It is worthy noting that the two hourly GIMs were linearly interpolated to hourly data using a similar approach as in Jee et al. (2010).

3   Single station model over Malindi

3.1   EOF decomposition of the TEC data

Empirical orthogonal function (EOF) analysis is a well-known method that dates back to the work of Pearson (1901), and has been widely used in climate (Hannachi et al., 2007) and ionospheric (Dvinskikh, 1988; Zhang et al., 2009; Liu et al., 2008) data analysis. It involves reducing the dimensionality of the data by finding a reduced set of variables (EOF modes or basis vectors) that explain most of the variability in the data. This allows for the original data (TEC(d, h)) to be expressed as a linear combination of a small number of basis functions as

$$\text{TEC}(d, h) = \sum_{j=1}^{n} U_j(h) \times C_j(d), \tag{1}$$

where C_j is the coefficient of the basis vector $U_j(h)$ with the index j running from 1 to n (the number of the retained EOF modes). We used the method of singular value decomposition (svd) to determine the EOF modes that explain most of the

3

variability in the TEC data. The TEC data matrix M was decomposed into U and V, the left and right basis vectors respectively, and S a matrix of singular values of M according to the equation

$$M = USV^T \tag{2}$$

The basis vectors of the first six EOF modes in matrix U and their corresponding coefficients obtained using equation 3 are
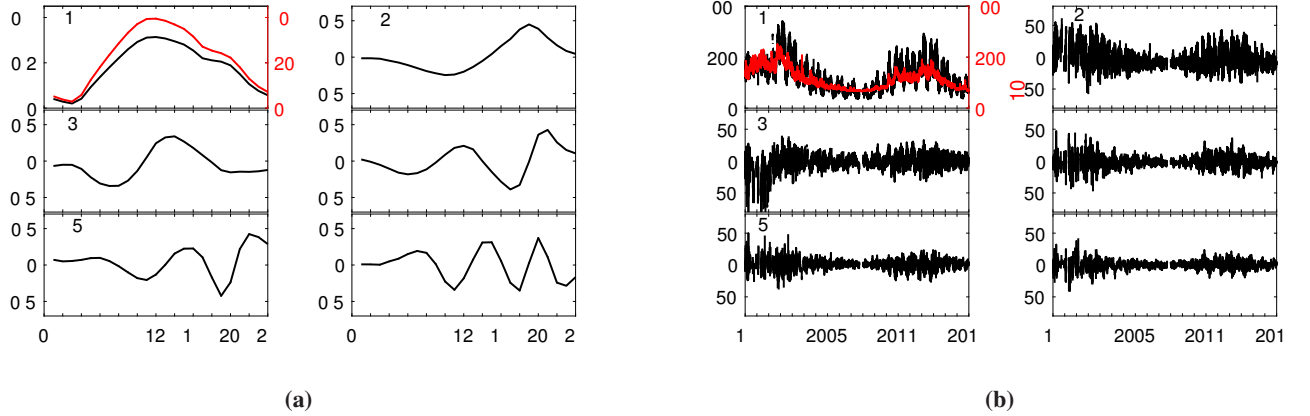

(a)   (b)

Figure 1. The first six basis functions (a) representing the diurnal variation and their coefficients (b) which show the long-term variation of TEC over MAL2. The red curves in the top left panels in (a) and (b) compare the diurnal mean TEC with the first basis vector U1 and the solar radio flux index measured at 10.7 cm wavelength (F10.7) with coefficients C1 of the first EOF mode respectively.

5   shown in Figure 1. While Table 1 shows the percentage variability in the data explained by the different EOF modes.

$$C_j(d) = S \times V_j^T \tag{3}$$

Figure 1 (a) shows that the average diurnal TEC (red curve) over Malindi has a pre-dawn minimum at about 03:00 UT, a

Table 1. Variance of the TEC data explained by the different EOF modes

EOF mode	1	2	3	4	5	6
Explained Var. (%)	96.8	1.0	0.8	0.3	0.20	0.1
Cumulative (%)	96.8	97.8	98.6	98.9	99.1	99.2

maxima at about 11:30 UT and an enhancement from 18:00 to 20:00 UT. The maxima at 11:30 UT is possibly due to increased ionization as the solar zenith angle is nearly zero over Malindi around this time. The post sunset increase in the TEC from 10   18:00 to 20:00 UT could be due to an enhancement in the eastward electric field before its westward reversal at night. Though the physical interpretation of the basis functions are normally difficult due to their geometric nature (Hannachi et al., 2007), the high correlation between the first basis mode U1 with the mean TEC shows that U1 is replicating the diurnal characteristics of the ionospheric TEC over Malindi. Figure 1 (b) shows that the semiannual and annual variations in TEC have peaks during the

equinoxes and high solar activity years respectively. These coefficients are well correlated with the solar radio flux measured at 10.7 cm wavelength (F10.7), confirming that the main driver of ionospheric variability over Malindi is the changes in the extreme ultraviolet (EUV) radiation from which the ionosphere owes its existence.

3.2 Modeling of the coefficients

5 Due to the rapid convergence of the basis functions, we used only the first six EOF modes which accounted for 99.2% of the explained variance in the data to model the observed regional TEC as derived from GNSS measurements at Malindi. For an effective TEC model, the choice of the input parameters to model the solar and magnetic activity dependences of the TEC is important. Table 2 shows the correlation coefficients for some of the commonly used solar and magnetic indices obtained from Omniweb[1] with the first six EOF coefficients. Among the solar indices, the first EOF coefficients showed stronger correlation

10 with the solar activity factor $F10.7_{av}$ (Richards et al., 1994; Liu et al., 2006) given by $F10.7_{av} = \frac{1}{2}(F10.7+F10.7_{81})$, where $F10.7_{81}$ is the 81 day average of F10.7 centered on the day of interest. For the magnetic indices, the first EOF coefficients showed the highest correlation with Dst followed by Kp and then AE. Based on the observations in Table 2, it was reasonable

Table 2. Correlation coefficients of some of the commonly used solar and magnetic indices with the first six EOF coefficients

EOF coeff.	Solar indices			Magnetic indices		
	Sunspot Number	F10.7	$F10.7_{av}$	Kp	AE	Dst
C1	71.2	75.8	79.1	19.0	15.6	-23.1
C2	36.6	35.	37.2	9.5	12.1	-5.5
C3	16.9	16.7	16.4	4.2	4.6	-4.1
C4	4.4	7.5	8.1	17.8	20.1	-13.3
C5	5.8	6.9	7.0	2.3	1.3	-6.8
C6	0.2	1.9	1.8	1.8	3.9	-4.4

to use F10.7av and Dst as inputs to model the solar and magnetic dependences of TEC over Malindi. Since Dst and F10.7av vary with the day of the year (DOY), our third input parameter was the DOY number. We then expressed the EOF coefficients

15 as a sum of linear and harmonic functions following the procedure of Zhang et al. (2009) as

$$C_j(d) = B_{j1}(d) + B_{j2}(d) + B_{j3}(d) \tag{4}$$

The term $B_{j1}(d)$ is to account for the linear variation of the EOF coefficients with solar and magnetic activities and is given by

$$B_{j1}(d) = a_{j1} + b_{j1} F10.7_{av}(d) + c_{j1} Dst(d) \tag{5}$$

[1]https://omniweb.gsfc.nasa.gov/

The semiannual and annual variations in the EOF coefficients are represented in equation 4 by the harmonic terms $B_{j2}(d)$ and $B_{j3}(d)$ of periods half a year and 1 year (365.25 days) respectively expressed as

$$B_{j2}(d) = \left[a_{j2} + b_{j2}F10.7_{av}(d) + c_{j2}Dst(d)\right]\cos\left(\frac{2\pi d}{365.25}\right) + \left[d_{j2} + e_{j2}F10.7_{av}(d) + f_{j2}Dst(d)\right]\sin\left(\frac{2\pi d}{365.25}\right) \quad (6)$$

$$B_{j3}(d) = \left[a_{j3} + b_{j3}F10.7_{av}(d) + c_{j3}Dst(d)\right]\cos\left(\frac{4\pi d}{365.25}\right) + \left[d_{j3} + e_{j3}F10.7_{av}(d) + f_{j3}Dst(d)\right]\sin\left(\frac{4\pi d}{365.25}\right) \quad (7)$$

The coefficients a_{j1} to f_{j3} in equations 5-7 were determined using a least squares fit to the EOF coefficients $C_j(d)$ in equation 3 obtained from GPS-derived TEC values measured at Malindi. The modeled TEC was then obtained using equation 1 by replacing the coefficients with their modeled values. The variation of the observed GPS-derived TEC, the reconstructed TEC from the first six EOF modes, and the modeled TEC are shown in Figure 2. It can be seen from Figure 2 a & b that the six EOF modes were sufficient to reproduce the variation in the TEC. Figure 2 c shows that the model quite well captured the diurnal, seasonal and the solar activity variations in the observed TEC over Malindi. Correlation analysis between the observed and the modeled TEC show a high positive correlation (Figure 2 d) with a correlation coefficient of 0.9225. This high correlation is an indication of the EOF decomposition method being capable of reproducing the inherent features of the dynamic ionosphere at the crest of the anomaly region. The reason for the positive bias of 3.2 TECU in the modeled TEC is not known.
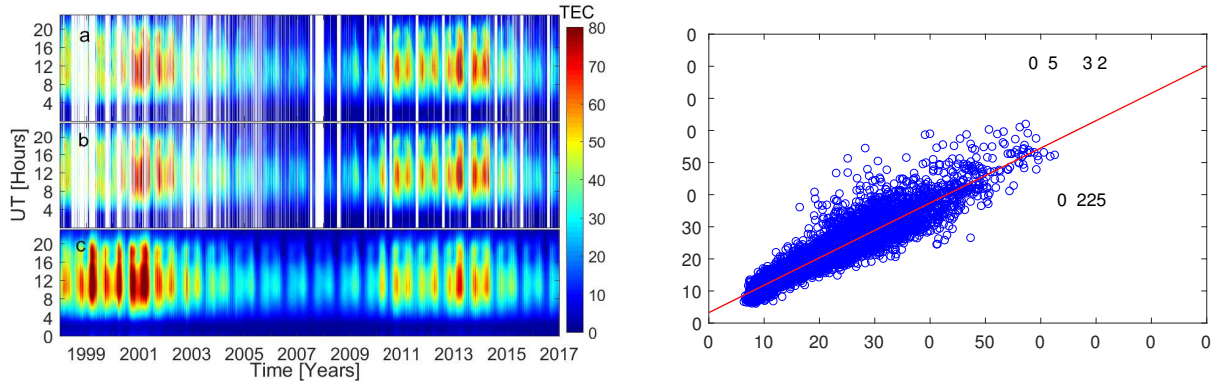

Figure 2. (a) GPS TEC, (b) reconstructed TEC and (c) modeled TEC over Malindi. (d) Correlation between EOF modeled TEC and GPS-derived TEC over Malindi from 1999 to 2017

3.3 Model validation

To asses the performance of the EOF-based TEC model, we compared the model results with the TEC derived from IRI-2016 model and GIMs obtained from the website[2] of Center for Orbit Determination in Europe (CODE). From here onwards, TEC from the EOF-based TEC model will be referred to as EOF TEC, TEC derived from the GPS receiver in Malindi as GPS TEC, TEC from CODE's GIMs as CODE's TEC and TEC from IRI-2016 model as IRI TEC. We used both Kp and Dst to characterize the days into quiet and disturbed. A day was considered to be quiet if Kp $\leq$3 for all 3-hour periods of the day.

3.3.1 Quiet days

Quiet days were selected from the equinox (March and September) and solstice (June and December) months of a high (2002) and low (2009) solar activity phases in order to validate the EOF-based TEC model. The data for the selected quiet days were excluded from the matrix used to generate the model coefficients, and the same procedure for model construction was repeated.

5   The IRI TEC for the selected days were obtained from the web interface of IRI-2016 model hosted at Omniweb[3]. To retrieve the IRI TEC, the location was specified to coincide with the geographic coordinates of MAL2 GPS receiver and the topside boundary was set to its maximum value of 2000 km. The NeQuick option was used as the topside electron density model and ABT-2009 for the bottom side thickness. Figure 3 shows hourly diurnal variation of GPS TEC, IRI TEC, EOF TEC and CODE's TEC over Malindi for some selected quiet days.

10   As expected, TEC values were higher in 2002 than in 2009. The IRI-2016 model overestimated the diurnal TEC over Malindi during the low solar activity year 2009 and during winter solstice of the high solar activity year 2002. The overestimate of the GPS TEC by the IRI TEC is similar to what Olwendo et al. (2012) observed when they compared GPS TEC measurements over Kenya with TEC from IRI-2007 model. During the equinox months of higher solar activity years, IRI TEC values were higher and lower than the GPS TEC at about 03:00-09:00 UT and 11:00-13:00 UT respectively. The CODE's TEC overestimated

15   the GPS TEC especially during the high solar activity year 2002. The overestimate of the GPS TEC by CODE's TEC was not much reflected during the low solar activity year 2009. The EOF TEC on the other hand replicated the diurnal TEC quite well except on DOY 066 and DOY 339 in 2009. In general, the highest correlation was observed between the GPS TEC and CODE's TEC followed by the correlation of the GPS TEC with the EOF TEC. It is worth noting that CODE's TEC mainly overestimated the TEC over Malindi especially during higher solar activity years. Meanwhile, the IRI-2016 overestimated the

20   GPS TEC over MAL2 between 03:00 and 07:00 UT during high solar activity periods, and throughout the day during lower solar activity years. This may be due to inadequate ingestion of ground based data from the East African region in to the IRI model. As earlier mentioned, measurements from ionosondes were used to provide ground data during IRI model construction, and such data is currently limited over East Africa.

3.3.2 Disturbed days

25   To study the storm time performance of the EOF-based TEC model, we simulated TEC for some selected geomagnetic storms. As stated earlier, the test days were excluded in the process of generating the model coefficients. The IRI TEC for the storm days were obtained with the storm model turned on. The bottom panels of Figure 4 show variation of the hourly diurnal TEC while the top panels show variation of Dst index during some selected major geomagnetic storms. In Figure 4 a, TEC variation for a storm that occurred from 29-30 October 2003 are shown. No continuous GPS TEC measurements were available from

30   MAL2 IGS receiver during this storm period. As can be seen in CODE's TEC, the storm had negative effect on the peak value of the TEC. The same negative storm effect was replicated by the EOF and IRI models especially on 30-31 October 2003. Another major geomagnetic storm occurred in December 2006 with the main phase on 15 December 2006 (Figure 4 b). The

---

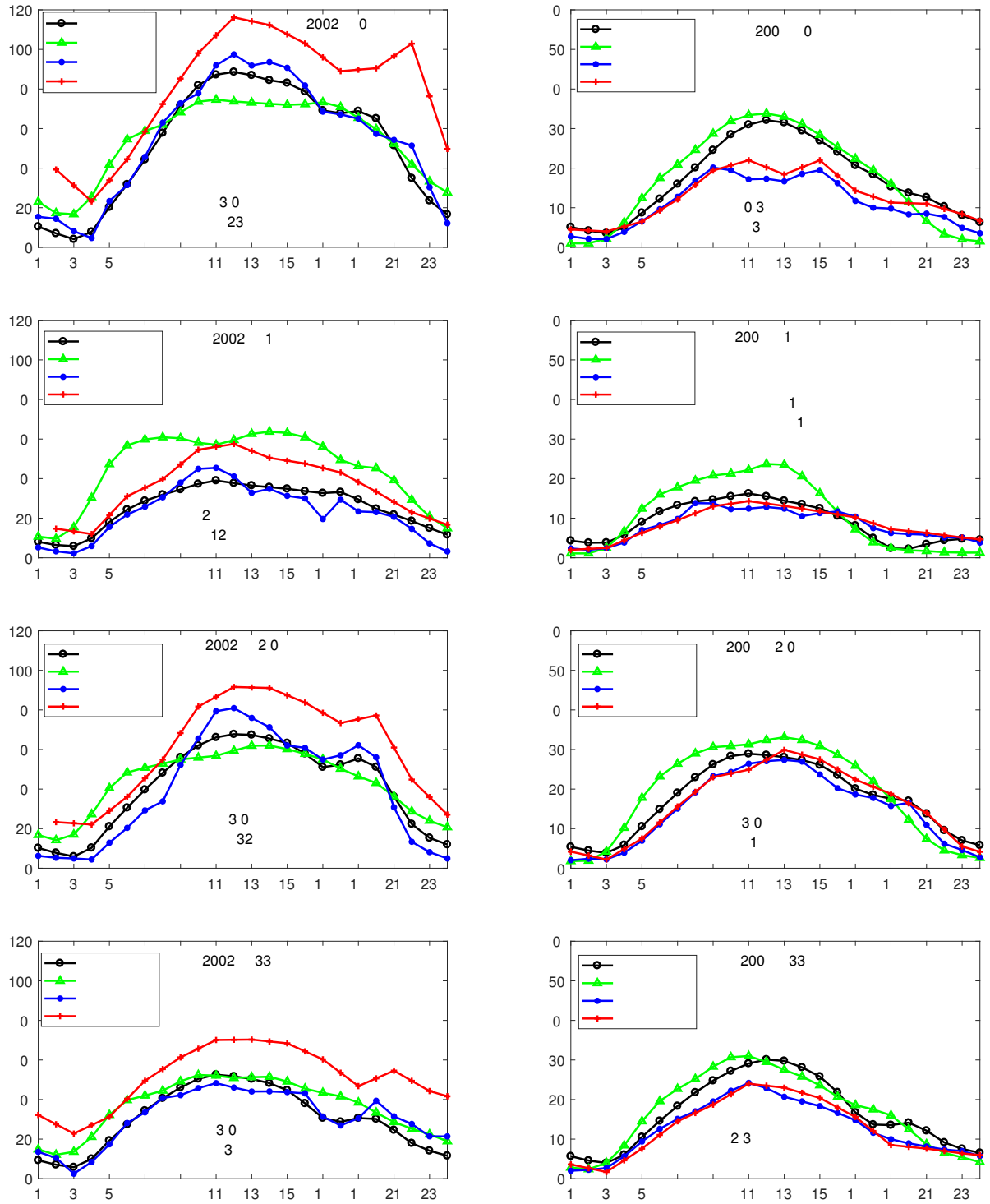[3]https://omniweb.gsfc.nasa.gov/vitmo/iri2016_vitmo.html

Figure 3. GPS TEC, IRI TEC, CODE's TEC and the EOF TEC over Malindi for some selected quiet days. Included in each plot are the maximum Kp and the minimum Dst index for the day.
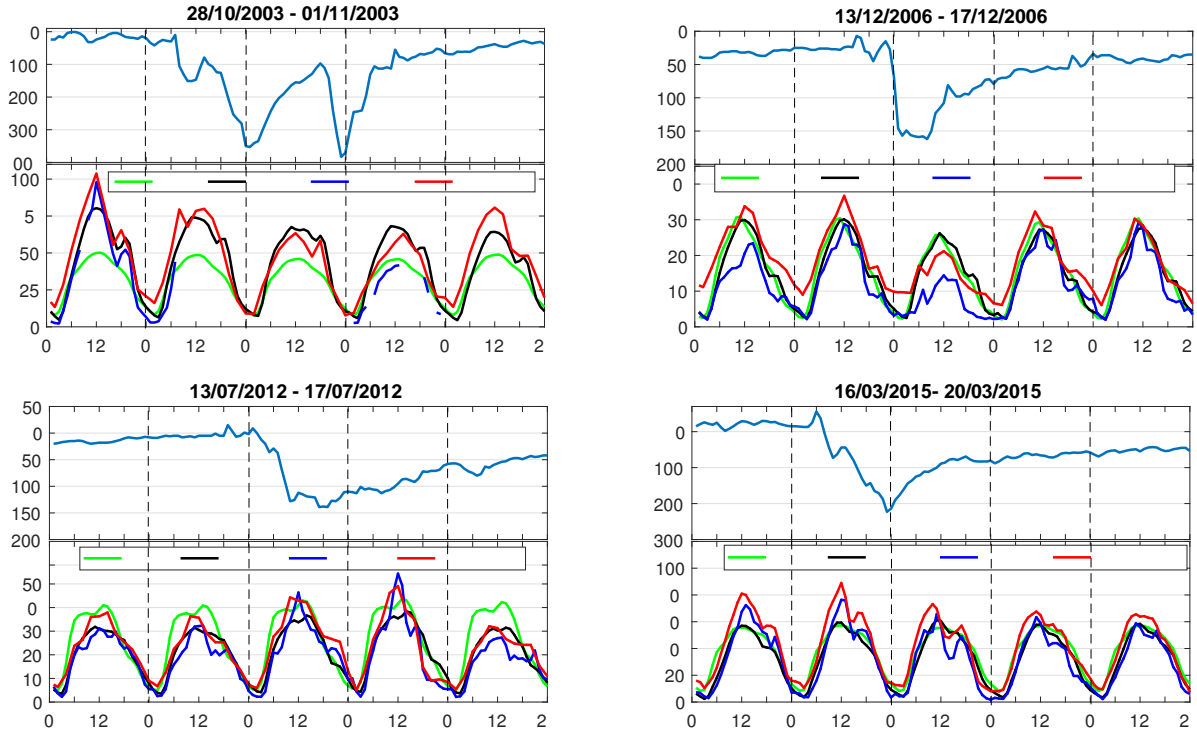
Figure 4. GPS TEC, IRI TEC, CODE's TEC and EOF TEC over Malindi for some selected storms. In these plots, the GPS TEC values are taken as a true representation of the ionosphere over Malindi. However, in the absence of GPS TEC (as in the case of the storm of 29-31 October 2003 shown in top left panel), CODE's TEC were taken as the correct description of the ionospheric response to the storm

EOF TEC, CODE's TEC and IRI TEC on the day of the main phase of the storm showed negative storm effects, consistent with the GPS TEC. A case of positive storm time effect on the ionosphere is shown in Figure 4 c where the EOF TEC and CODE's TEC showed similar positive storm time effect as in the GPS TEC. This was not reflected in the TEC derived from the IRI-2016 model. Shown in Figure 4 d is the TEC response to the geomagnetic storm that occurred in March 2015. During the recovery period which lasted for many days, the GPS TEC showed negative storm effects compared to its value during the time of storm commencement. The EOF TEC, CODE's TEC and IRI TEC all showed negative storm effects during the recovery period.

3.3.3 Statistical analysis

From the EOF-based TEC model, we have simulated TEC for the months of March, June, September and December for low (2009) and high (2013) solar activity years. In each of these simulations, the data for the selected months were excluded from the data used to generate the model coefficients. It is worthy noting that in generating the model coefficients, say for March

9

2009, it is only the data of March 2009 that was excluded. The monthly median values for the EOF TEC, IRI TEC and CODE's TEC were used to compute the root mean square error (rmse) of the predicted TEC from the GPS TEC for every hour of the day. The diurnal variation of the rmse values in 2009 and 2013 are shown in Figure 5. From Figure 5, the uncertainty in predicting
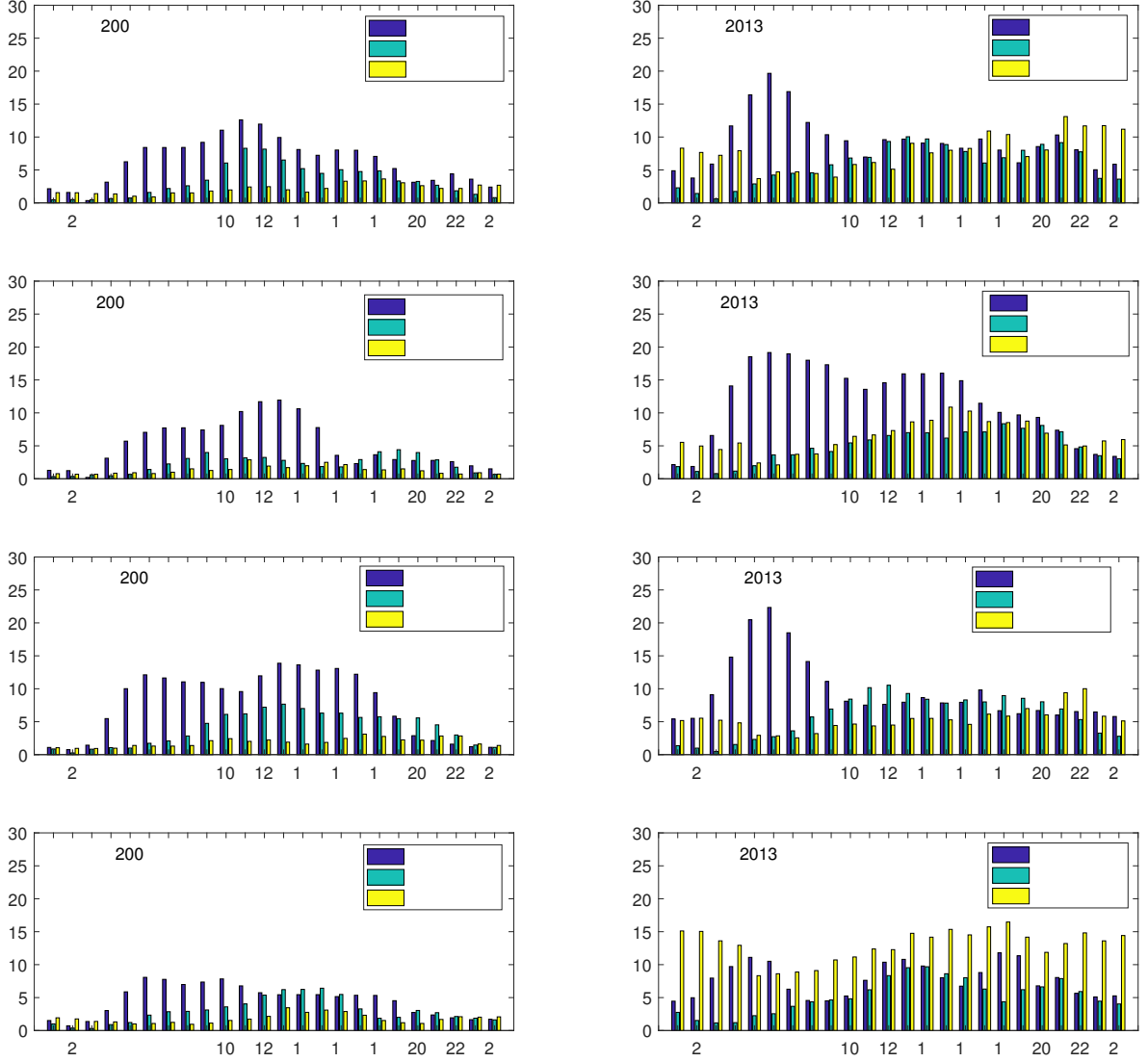

Figure 5. Diurnal variation of root mean square error (rmse) of IRI TEC, CODE's TEC and EOF TEC relative to GPS TEC over Malindi

the observed TEC was higher in 2013 than in 2009. This could be due to intensification of equatorial electrodynamic processes 5 and the associated effects such as TEC perturbations during higher solar activity years (Andima et al., 2015). These secondary effects of the equatorial dynamo processes are not probably well captured by the models. A comparison of the performance

of the different models has shown that, CODE's GIMs predicted the TEC over MAL2 with the least rmse values followed by the EOF model in 2009. The greatest uncertainty in predicting the TEC over MAL2 in the same year was observed in the IRI-2016 TEC. Similarly in 2013, the IRI TEC had higher rmse values compared to the EOF TEC. CODE's GIMs showed the largest uncertainty in predicting the TEC over MAL2 during December solstice of the high solar activity year 2013. The diurnal

5   uncertainties in the ability of IRI-2016 to predict the TEC over MAL2 exhibited two peaks in March, June and September in 2009. The maximum rmse values in the IRI-2016 predicted TEC were observed between 11:00 and 13:00 UT in March and June, and 13:00-14:00 UT in September in 2009. December solstice showed a single peak in the rmse values from 06:00-07:00 UT in 2009. Both the EOF TEC and CODE's TEC had the largest rmse values from 11:00-14:00 UT in the same year. The rmse values from 16:00-18:00 UT in March and September 2009 were quite higher than those in June and December of the same

10   year. In 2013, the rmse in the IRI-2016 predicted TEC in the months of March and September had only single peaks which occurred at about 06:00 UT. However, two peaks, one between 04:00 and 07:00 UT and second between 13:00 and 14:00 UT were observed in June and December 2013. The smallest error in the IRI TEC and the EOF TEC were observed after local midnight to about 03:00 UT in both 2009 and 2013.

4   Modeling TEC over African low latitudes

15   The first step in the regional TEC modeling was to extract the TEC for the African low latitude region from CODE's GIMs. The daily GIMs were organized into bins of $2.5^{\mathrm{o}} \times 5^{\mathrm{o}} \times 1$ Hr (latitude$\times$longitude$\times$LT). The binned data was then decomposed into the spatial and temporal components according to the equation

$$\text{TEC(lat, lon, LT, m)} = \sum_{i=1}^{r} U_i(\text{lon, lat}) \times P_i(\text{LT, m}) \tag{8}$$

In equation 8, U_i(lon, lat) are the basis modes representing the spatial TEC variability and P_i(LT, m) are the coefficients that

20   describe the temporal TEC variations in terms of local time (LT) and month (m). Figure 6 (a) shows the first four basis modes from the decomposition in equation 8, and their corresponding expansion coefficients are shown in Figure 6 (b). The first basis mode (Figure 6 (a) (i)) replicated the average TEC over African low latitude region for the period 1999-2017, and therefore represents the average TEC characteristics over Africa. This mode accounts for 97.012% of the TEC variability over the region. The coefficients of the first basis mode show that TEC over African low latitudes exhibits, diurnal, seasonal and solar activity

25   dependences (Figure 6 (b) (i)). Shown in Figure 6 (a) (ii) is the second basis mode and the coefficients of this mode are shown in Figure 6 (b) (ii). The second basis mode accounts for 1.255% of the total TEC variability and it demonstrates the TEC variability in the two hemispheres, possibly due to differences in the seasons in the two hemispheres. In Figure 6 (a) (iii), the effect of the magnetic and electric field coupling resulting in the EIA appears to be evident. This mode accounts for 0.455% of the total TEC variability over the African low latitude region.
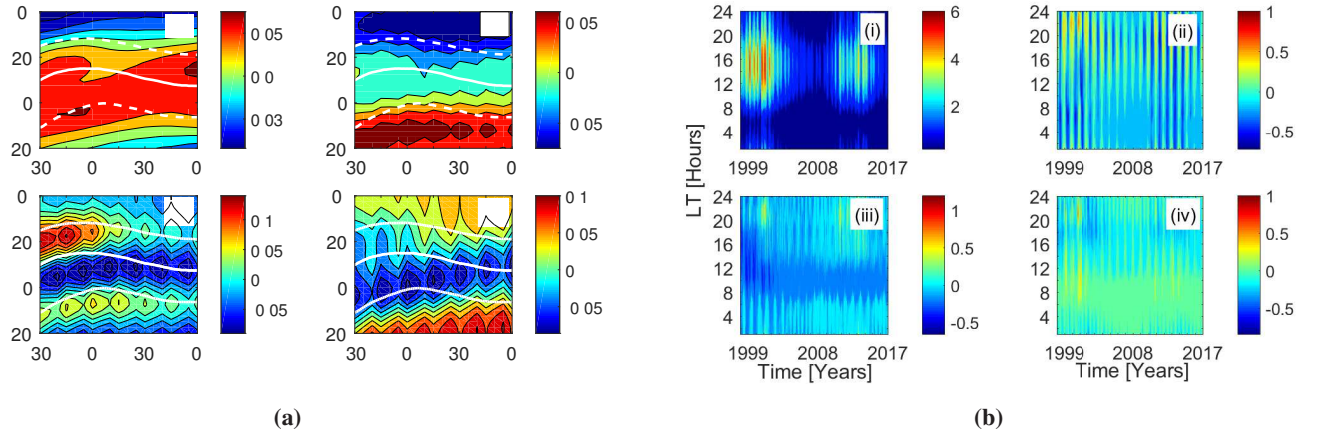
Figure 6. (a) The first four basis vectors from the first layer decomposition of the TEC data. (b) The coefficients of the basis modes in (a). The horizontal curved solid white lines in (a) show the geomagnetic dip equator. The dashed white lines show the anomaly region at $\pm 15^o$ geomagnetic latitude from the dip equator

The temporal component in equation 8 was further broken into the diurnal and long-term (seasonal, annual and solar cycle) variations by another decomposition which we refer to here as the second layer decomposition expressed as

$$P_i(LT, d) = \sum_{i,j=1}^{m} U_{i,j}(LT) \times A_{i,j}(d). \qquad (9)$$

In equation 9, $U_{i,j}(LT)$ are the basis functions of the ith first level coefficients and $A_{i,j}(d)$ are the coefficients of $U_{i,j}(LT)$. Figure 7 (a) show the first basis modes for each of the first four expansion coefficients in the first level decomposition. Equa-
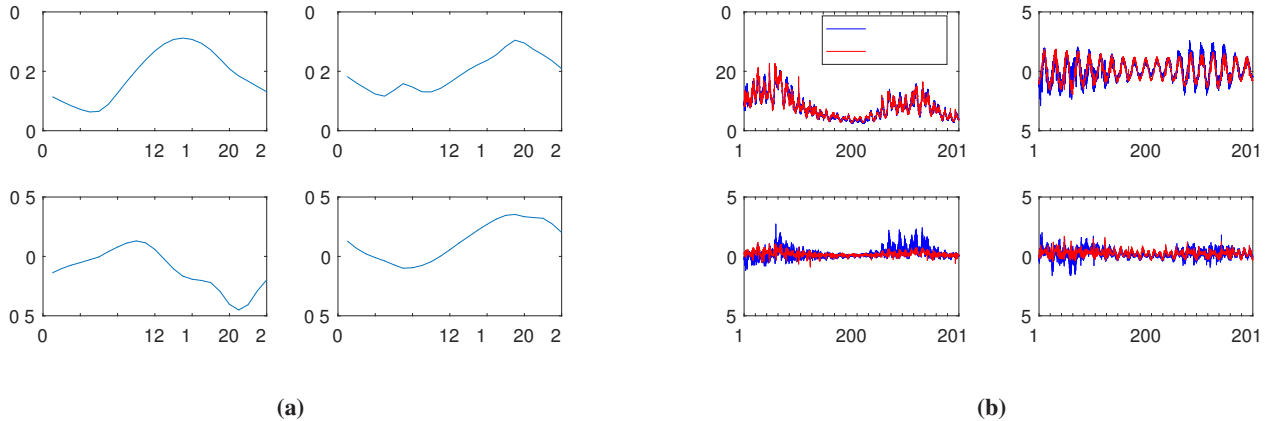

Figure 7. (a) The first basis modes of the first four first layer expansion coefficients. (b) The expansion coefficients (blue) and their modeled values (red) for the basis modes in (a).

5

tions 5 - 7 were then used to model the coefficients $A_{i,j}(d)$. Figure 7 (b) shows the coefficients $A_{i,j}(d)$ together with their model

predicted values. Using the modeled values of the coefficients, the regional TEC was then reconstructed in a reverse order. We first used equation 9 to obtain the coefficients for the first layer decomposition and then applied equation 8 to determine the TEC in each grid cell. Figure 8 shows the modeled TEC, CODE's TEC and IRI TEC for DOY 070 in 2015. It can be seen from Figure 8 that the model has quite well reproduced the main features of the EIA region. Higher correlations are observed

5   between EOF modeled TEC and CODE's TEC (Figures 8 a & b). This high correlation is an indication that the model predicted results could offer a good alternative in estimating background TEC since CODE's TEC are derived from GNSS measurements.
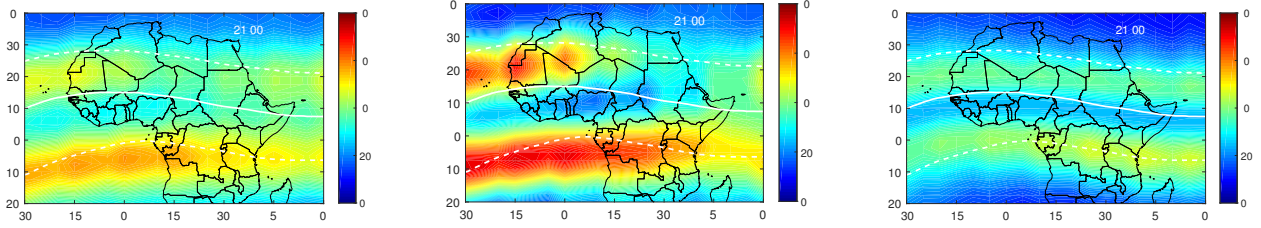

Figure 8. EOF TEC (a), CODE's TEC (b) and the IRI TEC (c) for the DOY 070 in 2015. Shown on the plots are the local times in hours. The horizontal curved white lines are same as described in Figure 6.

5   TEC trends

In the past, few studies (e.g Lean et al. 2011; Lastovicka et al. 2017) have derived long-term TEC trends, and these mainly used

10   TEC data from GIMs. In this work, we have used GPS-derived TEC and GIMs to study TEC trends over the low latitude region of Africa. A key aspect in trend studies is the art of suppressing the solar and magnetic activity influences on these trends. We used the EOF modeled TEC as background TEC to remove the solar and magnetic effects in influencing the TEC trends. First, the monthly median TEC values were calculated from the daily TEC. The median TEC values were then modeled using similar equations as in equations 5−7. In these equations, the daily inputs were replaced with their monthly averages. The modeled

15   TEC values were then subtracted from the monthly medians to obtain the TEC residuals. The monthly TEC residuals from 10:00-14:00 LT were averaged for each year to give a representation of the noontime annual TEC residuals (ΔTEC). The trend was then determined using the equation (Lastovicka et al., 2006; Bremer et al., 2012).

$$\Delta TEC = A + B * time \ (year) \tag{10}$$

where A is the constant part and B the slope (trend) of the time-dependent TEC residuals. Lastovicka et al. (2017) attributed the

20   positive global TEC trends reported in Lean et al. (2011) to lower TEC values in CODE's GIMs especially prior to 2003. To test this assertion, we have estimated the long-term trends in TEC for the periods 1999-2017 and 2003-2017 using GPS-derived TEC, CODE's TEC and TEC from IGS GIMs. Figure 9 shows the TEC trends obtained from GPS-derived TEC and TEC from GIMs of CODE and IGS over Malindi. Trends of 0.139±0.063 TECU/year, -0.119±0.061 TECU/year and -0.057±0.042
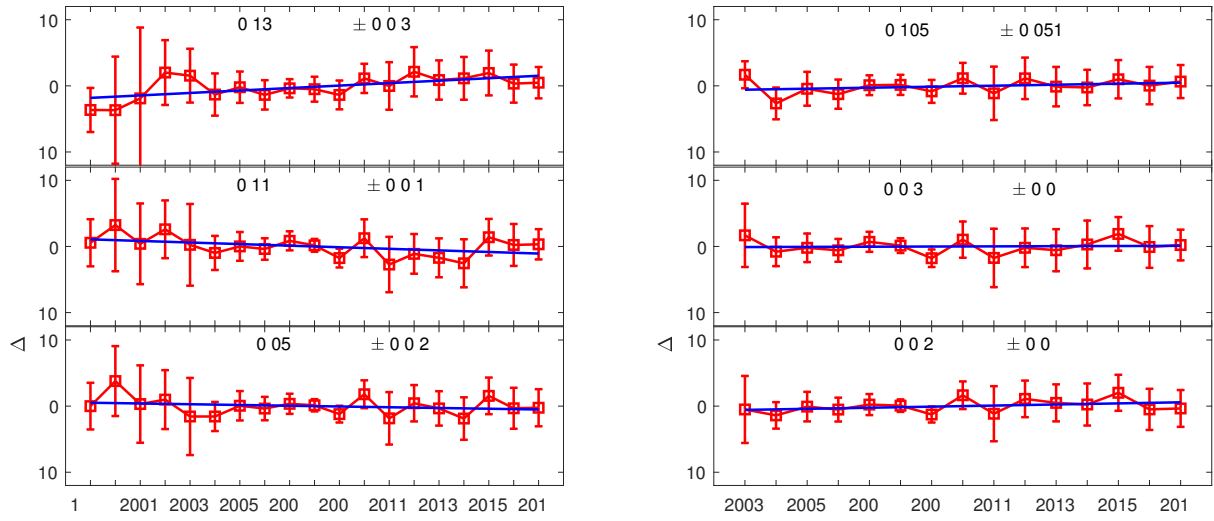
Figure 9. The yearly median residual TEC after removing the solar and magnetic activity variations for the periods 1999-2017 (a) and 2003-2017 (b). The upper panels are for the TEC derived from MAL2 IGS receiver, the middle panels are for TEC from CODE's GIMs and the lower panels are for TEC from IGS's GIMs corresponding to the location of MAL2 IGS receiver. The straight lines in these plots are the first degree polynomial fits used to estimate the trends

TECU/year were obtained using the GPS TEC, CODE's GIMs and IGS GIMs over Malindi respectively. Though the trend values in Figure 9a were slightly different, their 95% confidence bounds reveal a slight positive TEC trend for the period 1999-2017. For the period 2003-2017, the trend estimates from the three data sets show that TEC trends over MAL2 are positive. To study the trends in TEC over the African low latitude region, we used the GIMs and estimated the trends in each of the $2.5^{o} \times 5^{o}$
5   (latitude$\times$longitude) grids. The trends are shown in Figure 10(a) and (c) for the period 1999-20017 and in Figure 10(b) and (d) for the period 2003-2017. The trends in Figure 10 show a latitudinal dependence with the trends in the vicinity of the crest of the EIA region being more positive than those near the magnetic equator, where the trend was negative over most of the African equatorial region. Analysis of the data from 1999-2017 revealed higher average value of TEC trends than that from 2003-2017 for both CODE's and IGS GIMs, though the general pattern of the trends remained unchanged. The trend pattern observed in
10   this study confirm the latitudinal variation in TEC trends reported in Lean et al. (2011). The difference in the trend magnitudes for the periods 1999-2017 and 2003-2017 could be as pointed out earlier due to a bias towards lower values of GIMs prior to 2002 (Lastovicka et al., 2017; Emmert et al., 2017). If so, the trends in TEC over African low latitudes are therefore mainly negative, though cases of slight positive trends are also possible especially at the crest of the EIA region. Geomagnetic or anthropogenic factors are often the plausible physical mechanisms to explain trends in upper atmospheric parameters. The
15   anthropogenic contributions to trends arises through the accumulation of greenhouse gases which result in decrease of atomic oxygen in the upper atmosphere. Some authors (e.g Danilov and Mikhailov 1999; Mikhailov 2008) attribute the geomagnetic
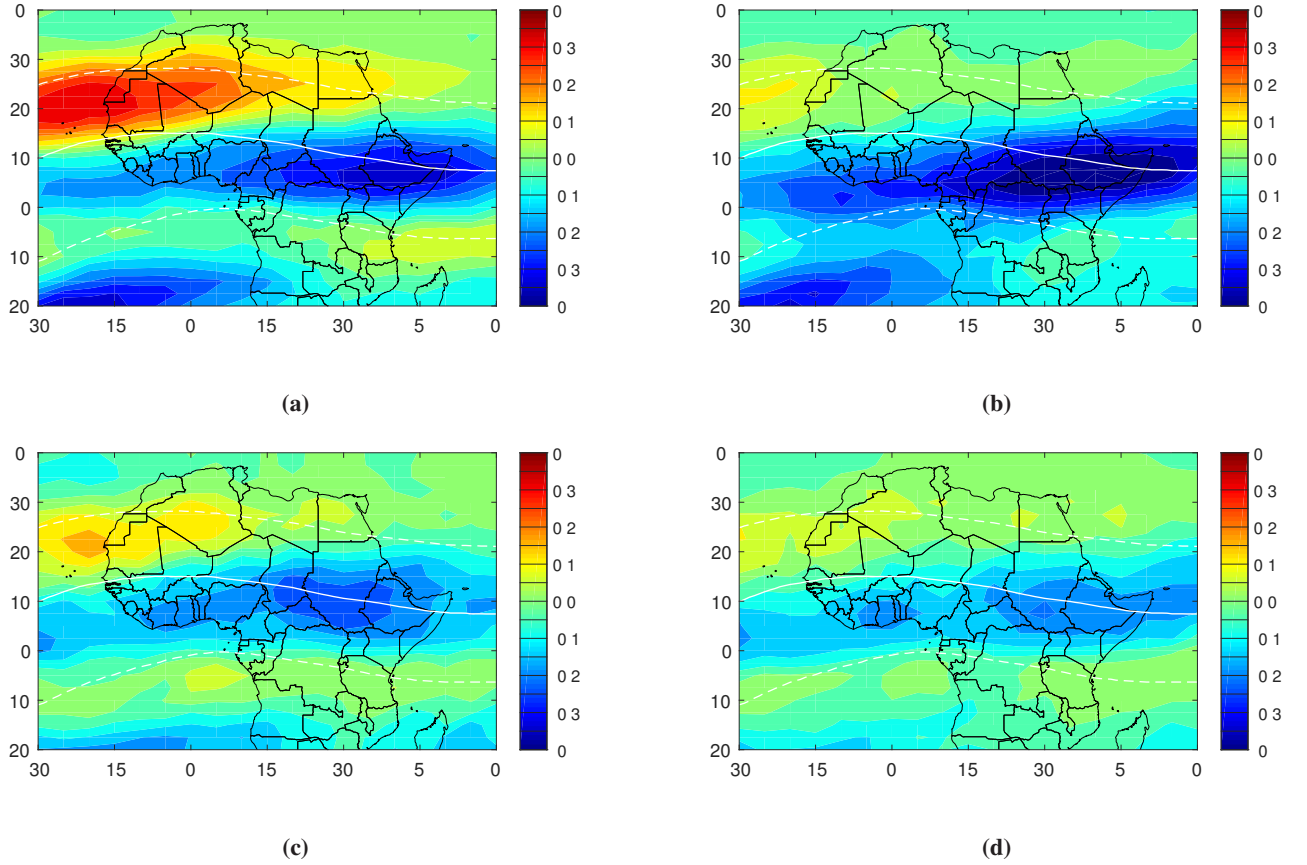
14

Figure 10. Trends in TEC over the African low latitude region derived from CODE's ((a) and (b)) and IGS's ((c) and (d)) GIMs. (a) and (c) are for the period 1999-2017 while (b) and (d) are for the period 2003-2017. The horizontal curved white lines are same as described in Figure 6.

control of the trend to geomagnetic storms that result in compositions changes which in turn affect ionospheric currents. This latter view may explain the latitudinal dependence in the trends over African low latitude region.

6 Summary and Conclusion

We have used EOF expansion together with least square regression to model TEC over the African low latitude region. We first developed a single station model over MAL2, a station at the southern crest of the EIA, and then constructed a regional model to predict TEC over the African low latitudes. Despite the complicated nature of the low latitude ionosphere, the model over MAL2 was able to satisfactorily reproduce the diurnal, seasonal and solar activity variations in the observed TEC. Comparison of the model results with IRI-2016 derived TEC showed that the EOF-based TEC model was more accurate in predicting the daytime TEC over Malindi than IRI-2016. On the other hand, CODE's GIMs were better correlated with GPS TEC than

the TEC from the EOF-based model, though CODE's GIMs mainly overestimated the GPS TEC over MAL2 during higher solar activity years. The large discrepancy of the IRI-2016 predicted daytime TEC from the observed TEC over MAL2 during periods of low solar activity and during the winter solstice could be due to over representation of the effects of the low latitude E×B plasma drifts and thermospheric winds in the model. The regional model reproduced quite well the known features of the low latitude ionosphere. Using the TEC from the EOF-based model as background TEC to suppress solar and magnetic activity dependence of TEC, we estimated trends in TEC over the African low latitude region. The regional trends showed a latitudinal dependence with the trends in the vicinity of the magnetic equator being more negative than those at the crest of the EIA.

References

Adewale, A. O., Oyeyemi, E. O., Adeloye, A. B., Ngwira, C. M., and Athieno, R.: Responses of equatorial F region to different geomagnetic storms observed by GPS in the African sector, J. Geophys. Res., 116, A12 319, 2011.

Anderson, D. N., Mendillo, M., and Herniter, B.: A semi-empirical low-latitude ionospheric model, Radio Sci., 22, 292–306, 1987.

5 Andima, G., Jurua, E., Amabayo, E. B., and Habarulema, J. B.: Statistical analysis of TEC perturbations over a low latitude region during 2009-2013 ascending solar activity phase, Adv. space Res., 56, 2542–2551, 2015.

Appleton, E. V.: Two Anomalies in the Ionosphere, Nature, 157, https://doi.org/10.1038/157691a0, 1946.

Bencze, P.: Some results referring to the long-term change of ionospheric parameters, Acta Gead. Geaph. Hung, 37, 403–408, 2002.

Bencze, P.: On the long-term change of ionospheric parameters, J. Atmos. Sol.-Terr., 67, 1298–1306, 2005.

10 Bilitza, D.: International reference ionosphere 1990, National Space Science Data Center, 26, 1990.

Bremer, J., Damboldt, T., Mielich, J., and Suessmann, P.: Comparing long-term trends in the ionospheric F2-region with two different methods, J. Atmos. Sol.-Terr., 77, 174–185, 2012.

Chen, Z., Zhang, S.-R., Coster, A. J., and Fang, G.: EOF analysis and modeling of GPS TEC climatology over North America, J. Geophys. Res.: Space Physics, 120, 3118–3129, 2015.

15 Danilov, A. D. and Mikhailov, A. V.: Spatial and seasonal variations of the foF2 long-term trends, Ann. Geophys., 17, 1239–1243, 1999.

Dvinskikh, N. I.: Expansion of ionospheric characteristics fields in empirical orthogonal functions, Adv. space Res., 8, 179–187, 1988.

Elias, A. G.: Possible Sources of Long-Term Variations in the Mid-Latitude Ionosphere, J. Open Atmos. Sci., 5, 9–15, 2011.

Emmert, J. T., Mannucci, A. J., McDonald, S. E., and Vergados, P.: Attribution of interminimum changes in global and hemispheric total electron content, J. Geophys. Res. Space Physics, 122, 2424–2439, 2017.

20 Ercha, A., Zhang, D., Ridley, A. J., Xiao, Z., and Hao, Y.: A global model: Empirical orthogonal function analysis of total electron content 1999–2009 data, J. Geophys. Res., 117, A03 328, 2012.

Habarulema, J. B., McKinnell, L.-A., Burešovà, D., Zhang, Y., Seemala, G., Ngwira, C., Chum, J., and Opperman, B.: A comparative study of TEC response for the African equatorial and mid-latitudes during storm conditions, J. Atmos. Sol.-Terr., 102, 105–114, 2013.

Hajra, R., Chakraborty, S. K., Tsurutani, B. T., DasGupta, A., Echer, E., Gonzalez, C. G. B. A. W. D., and Sobral, J. H. A.: An empirical
25 model of ionospheric total electron content (TEC) near the crest of the equatorial ionization anomaly (EIA), J. Space Weather Space climate, 6, A29, 2016.

Hannachi, A., Jolliffe, I. T., and Stephenson, D. B.: Empirical orthogonal functions and related techniques in atmospheric science: A review, International journal of climatology Int. J. Climatol. 27: (2007), 27, 1119–1152, 2007.

Hernandez-Pajares, M., Juan, J. M., Sanz, J., Orus, R., Garcia-Rigo, A., Feltens, J., Komjathy, A., Schaer, S. C., and Krankowski, A.: The
30 IGS VTEC maps: a reliable source of ionospheric information since 1998, J. Geod., 83, 263–275, 2009.

Jarvis, M. J., Jenkins, B., and Rodgers, G. A.: Southern hemisphere observations of a long-term decrease in F region altitude and thermospheric wind providing possible evidence for global thermospheric cooling, J. Geophys. Res., 103, 20 774–20 787, 1998.

Jee, G., Lee, H. B., Kim, Y. H., Chung, J. K., and Cho, J.: Assessment of GPS global ionosphere maps (GIM) by comparison between CODE GIM and TOPEX/Jason TEC data: Ionospheric perspective, J. Geophys. Res., 115, A10 319, 2010.

35 Kelley, M. C.: The Earth's ionosphere: Plasma Physics and Electrodynamics, Amsterdam, academic Press, second edn., 2009.

Kersley, L., Malan, D., Pryse, S. E., Cander, L. R., Bamford, R. A., Belehaki, A., Leitinger, R., Radicella, S. M., Mitchell, C. N., and Spencer, P. S.: Total electron content-A key parameter in propagation: measurement and use in ionospheric imaging, Ann. Geophysics, 47, 1067–1091, 2004.

Lastovicka, J.: Are trends in total electron content (TEC) really positive, J. Geophys. Res.: space physics, 118, 3831–3835, 2013.

5   Lastovicka, J., Mikhailov, A., Ulich, T., Bremer, J., Elias, A., de Adler, N. O., Jara, V., del Rio, R. A., Foppiano, A., Ovalle, E., and Danilov, A.: Long-term trends in foF2: A comparison of various methods, J. Atmos. Sol.-Terr., 68, 1854–1870, 2006.

Lastovicka, J., Urbar, J., and Kozubek, M.: Long-term trends in the total electron content, Geophys. Res. Let., 44, 8168–8172, https://doi.org/10.1002/2017GL075063, 2017.

Lean, J. L., Emmert, J. T., Picone, J. M., and Meier, R. R.: Global and regional trends in ionospheric total electron content, J. Geophys. Res.,
10   116, A00H04, 2011.

Liu, C., Zhang, M.-L., Wan, W., Liu, L., and Ning, B.: Modeling M(3000)F2 based on empirical orthogonal function analysis method, Radio Sci., 43, RS1003, 2008.

Liu, L., Wan, W., Ning, B., Pirog, O. M., and Kurkin, V. I.: Solar activity variations of the ionospheric peak electron density, J. Geophys. Res., 111, A08 304, 2006.

15   Martyn, D. F.: Atmospheric Tides in the Ionosphere. I. Solar Tides in the F_2 Region, Proc. R. Soc. Lond. Series A, 189, 241–260, https://doi.org/10.1098/rspa.1947.0037, 1947.

Mikhailov, A. V.: Ionospheric F1 layer long-term trends and the geomagnetic control concept, Ann. Geophys, 26, 3793–3803, 2008.

Moffett, R. J.: The equatorial anomaly in the electron distribution of the terrestrial F-region, Fund. Cos. Phy., 4, 313–391, 1979.

Olwendo, O., Cilliers, P., Baki, P., and Mito, C.: Using GPS-SCINDA observations to study the correlation between scintillation, total
20   electron content enhancement and depletions over the Kenyan region, Adv. space Res., 49, 1363–1372, 2012.

Pearson, K.: On lines and planes of closest fit to systems of points in space, Philos. Mag, 2, 559–572, 1901.

Rawer, K. and Bilitza, D.: International reference ionosphere-plasma densities: status 1988, Adv. space Res., 10, (8)5—(8)14, 1990.

Reinisch, B. W., Huang, X., Belehaki, A., Shi, J. K., Zhang, M. L., and R.Ilma: Modeling the IRI topside profile using scale heights from ground-based ionosonde measurements, Adv. space Res., 34, 2026–2031, 2004.

25   Richards, P. G., Fennelly, J. A., and Torr, D. G.: IEUVAC:A solar EUV flux model for aeronomic calculations, J. Geophys. Res., 26, 8981–8992, 1994.

Seemala, G. K. and Valladares, C.: Statistics of total electron content depletions observed over the South American continent for the year 2008, Radio Sci., 46, RS5019, https://doi.org/doi:10.1029/2011RS004722, 2011.

Zhang, M. L., Liu, C., Wan, W., Liu, L., and Ning, B.: A global model of the ionospheric F2 peak height based on EOF analysis, Ann.
30   Geophys., 27, 3203–3212, 2009.